Thesis for the degree of Licentiate of Engineering

Design and Optimization of Wideband Hat-Fed Reflector Antenna with Radome for Satellite Earth Station

by

Erik G. Geterud

CHALMERS

Department of Signals and Systems
Chalmers University of Technology
Göteborg, Sweden 2012

Göteborg 2012

Design and Optimization of Wideband Hat-Fed Reflector Antenna with Radome for Satellite Earth Station

Erik G. Geterud

This thesis has been prepared using LaTeX.

Copyright © Erik G. Geterud, 2012.
All rights reserved.

Department of Signals and Systems
Technical Report No. R013/2012
ISSN 1403-266X

Department of Signals and Systems
Antenna Group
Chalmers University of Technology
SE-412 96 Göteborg, Sweden

Phone: +46 (0)31 772 0000
E-mail: erik.geterud@chalmers.se

Printed by Chalmers Reproservice
Göteborg, Sweden, September 2012

To my parents

Abstract

This thesis presents the development of a hat-fed reflector antenna with radome to be used as satellite earth station. The antenna with self supported feed is relatively compact, circular symmetric and with low cross polarization. To achieve optimum performance over the satellite Ku-band, covering 10.75-14.50 GHz, a genetic algorithm optimization scheme was implemented and the simulations were done with the electromagnetic solver QuickWave-V2D based on the FDTD method. Optimizations were done towards minimized reflection coefficient, maximized feed efficiency, and finally taking into account the stringent sidelobe requirements defined by the ETSI. Radomes for enclosing the satellite earth station have been analyzed and a low loss monolayer radome was manufactured and successfully measured with the hat-fed reflector antenna. The satellite earth station can after certification be operational.

Keywords: Antenna feeds, corrugated surfaces, reflector antennas, optimization, radomes, satellite earth stations.

Preface

This thesis is in partial fulfillment for the degree of Licentiate of Engineering at Chalmers University of Technology.
The work resulting in this thesis was done between April 2008 and August 2012. I have during the licenciate period been an external industrial Ph.D. student fully employed by GlobalView Systems Sweden. The work has been done in close collaboration with the Antenna department at Arkivator AB and the Antenna Group, in the Department of Signals and Systems, at Chalmers in Göteborg. Professor Per-Simon Kildal is the examiner and Associated Professor Jian Yang is the supervisor.

List of Publications

This thesis is based on the work contained in the following papers:

Paper I
E. G. Geterud, Y. Yang and T. Östling, "Wide band hat-fed reflector antenna for satellite communications", in *Proceedings of the 5th European Conference on Antennas and Propagation, EUCAP 2011, Rome, Italy, 11-15 April 2011.*

Paper II
E. G. Geterud, Y. Yang and T. Östling, "Radome design for hat-fed reflector antenna", in *Proceedings of the 6th European Conference on Antennas and Propagation, EuCAP 2012, Prague, Czech Republic, 26-30 March 2012.*

Paper III
E. G. Geterud, Y. Yang, T. Östling and P. Bergmark, "Design and Optimization of a Compact Wideband Hat-Fed Reflector Antenna for Satellite Communications", *IEEE Transactions of Antennas and Propagation, to be published.*

Other related publications by the Author not included in this thesis:

- E. G. Geterud, M. Hjelm, T. Ciamulski and M. Sypniewski "Simulation of a lens antenna using a parallelized version of an FDTD simulator", in *Proceedings of the 3rd European Conference on Antennas and Propagation, EUCAP 2009, Berlin, Germany, 23-27 March 2009.*

Acknowledgements

First of all I would like to thank my examiner Professor Per-Simon Kildal, for accepting me as an industrial Ph.D. student in the Antenna group, and my supervisor Associated Professor Jian Yang. Both have been supportive and we had many fruitful technical discussions.

Also, without the strong and long term support from GlobalView Systems including my colleague Matthew Wright my research at Chalmers could never have been realized.

Thanks goes to Tomas Östling at Arkivator for support with the GA optimization and hardware including the hat feed, reflector antenna and radome. I must also mention Dr Pontus Bergmark at Art and Technology for his crafting of radome prototypes and free-thinking spirit. Raul Timbus from Ruag Space has taken many Ph.D. courses with me and we had many enjoyable discussions on antennas and other topics. Thanks also to Marie Ström in the Signal Processing group for keeping me in shape through lunch climbing sessions in Kopparbunken.

I would like to thank all past and present members of the antenna group at Chalmers for creating an enjoyable working environment. The yearly ski trip arranged by Per-Simon has been an appreciated event with team building exercises and lots of fun. Also the whole department of Signals and Systems are acknowledged for creating a good atmosphere and arranging many enjoyable social events.

Erik

Göteborg, August 2012

Contents

Part I
Introductory chapters

Chapter 1

Introduction

The developed satellite earth station in this work is for communication with geosynchronous satellites and in this first part a short introduction to the intriguing topic of satellite communication is given. The notion of a geosynchronous satellite for communication purposes was first published in 1928 (but not widely so) by the Austro-Hungarian rocket engineer and pioneer of cosmonautics Herman Potocnik (Noordung) [1]. The idea of satellite communication (satcom) was later made popular in 1945 by British science fiction author, inventor, and futurist Arthur C. Clarke [2] but it was not until the launch of the Sputnik Satellite in 1957 that this idea was considered realistic. The first communication satellite Telstar was launched in 1962 and since then numerous satellites have been launched with ever increasing sophistication. A communication satellite is a microwave repeater station that permits two or more users with appropriate earth stations to deliver or exchange information of various forms [3]. The satellite is composed of three separate units being the fuel system, the satellite and telemetry controls and the transponder. The transponder includes antennas, receivers, input multiplexers, and a frequency converter which is used to reroute the received signals through a high powered amplifier for downlink [3]. The main task for a telecom satellite is to receive signals from earth stations and to relay them over a specific geographical area defined by the spotbeam of the transmitting satellite antenna. The communication link can be bi-directional as for satellite telephony etc. For Earth observation the satellite is equipped with cameras and sensors and downlinks the collected information. The Earth station may operate uplink in transmitting mode (Tx) and/or downlink in receiving mode (Rx). In case of uplink the transmitting station sends data in the form of baseband signals, which passes through a baseband processor, an up converter, a high powered amplifier, and through the antenna to the satellite. The reverse process is

valid in receive mode. A scenario of satellite communications with various earth terminals is shown in Figure 1.1.

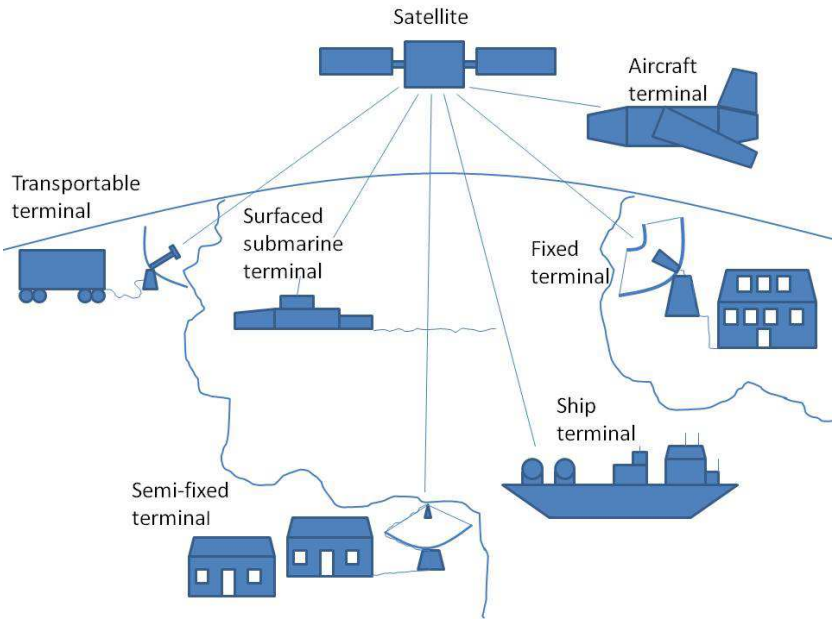

Figure 1.1: Satellite communications scenario.

The Geostationary Earth Orbit (GEO) refers to satellites that are placed in orbit such that they remain stationary relative to a fixed spot on earth. The satellites are placed at 35,786 km above the earth surface along the equator, and its angular velocity is equal to that of the earth, thereby causing it to appear to be over the same point on earth. This allows for them to provide constant coverage of the area e.g. for television broadcasting. The distance from an earth station positioned at the equator to a geosynchronous satellite in zenith is 35,786 km which introduces a propagation delay of approximately a quarter of a second when relaying a signal between two users on earth. Due to this time delay, bi-directional communications, are preferably done via lower orbiting satellites. This is the case for omni-directional antennas and low data rates when no satellite tracking is required.

Medium Earth orbit (MEO), sometimes called intermediate circular orbit (ICO), is the region of space around the Earth above low Earth orbit (altitude of 2,000 km) and below geostationary orbit (altitude of 35,786 km). The orbital periods of MEO satellites range from about 2-12 hours and the dominating use is for positioning with GPS, Glonass and Galileo satellites.

The Low Earth Orbit (LEO), refers to satellites in orbit 160-2,000 km above the earths surface which reduces transmission times. A LEO orbit

can also be used to cover a polar region, which the GEO cannot. Since the satellites do not appear stationary to earth stations the antenna may need to track the motion of the satellite. The most striking LEO satellite is arguably the International Space Station (ISS) which orbit varies from 320-400 km above the Earth's surface.

The main satellite communication bands being:

- L-band, 1-2 GHz (GPS frequencies: 1.575 GHz L1, 1.228 GHz L2)
- S-band, 2-4 GHz (Weather- and surface ship radar and ISS space shuttle telecom)
- C-band, 4-8 GHz (Satcom bands: 3.400-3.625 GHz Rx, 6.425-6.725 Tx)
- X-band, 8-12 GHz (Military radar and deep space telecom)
- Ku-band, 12-18 GHz (Satcom bands:10.70-12.75 GHz Rx, 13.75-14.50 GHz Tx)
- K-band, 18-26.5 GHz (Satcom band:17.70-20.20 GHz Rx)
- Ka-band, 26.5-40 GHz (Satcom band: 27.50-30.00 GHz Tx)

In this thesis we present an earth station for communication with geostationary satellites in the form of a hat-fed reflector antenna with radome. The antenna design is for the Ku-satcom-band which cover a 1.3:1 bandwidth which is a challenging task in terms of reflection coefficient and the stringent sidelobe requirements. The antenna and feed electronics needs to be enclosed by a radome to protect from harsh environment such as rain, snow, dust and wind. The radome must be low loss and designed in conjunction with the antenna to ensure satisfactory electromagnetic performance. Simulations and optimization techniques are used in order to fulfill the requirements on co- and cross-polar radiation patterns, reflection coefficient and efficiency.

1.1 Aim and Outline of the Thesis

The aim of this thesis work is to develop and optimize a wideband hat-fed reflector antenna satellite earth station with radome. Previously, the hat feed has been used in terrestrial radio links and gauge radars etc. The bandwidth is narrow but encouraging work has been done towards wideband solutions [4]. In this work we need to extend the bandwidth further by implementing optimization schemes in conjunction with an electromagnetic solver. If

successful it will be the first hat-fed reflector antenna used for satcom applications [5, 6] and a more compact solution than other reflector configurations available on the market . The radome is a critical component in the satellite earth station and it must be robust and low loss [7].
This thesis is separated in two main parts. The first part introduces the subject and is divided as follows: Chapter 2 provides an overview of available antenna technologies for satellite communications and the selected topology is motivated. Chapter 3 introduces the electromagnetic solver used and the optimization technique. Chapter 4 presents the hat feed and its characteristics with Gaussian vertex plate, Antenna Noise Temperature and G/T factor. Chapter 5 introduces radomes including evaluation of monolayer- and sandwich structures. Chapter 6 includes a description of the development work done and summarizes the appended papers. Chapter 7 ends the first part of the thesis with conclusions and future work. In the second main part, the contributions from the author are included as three appended papers.

Chapter 2

Antenna Technologies for Satellite Earth Stations

2.1 Reflector Antennas

Reflector antennas for microwaves evolved from the attempts to increase the directivity of half wave dipoles using sheet reflectors [8]. Reflector antennas are today the most used antenna technology for satellite earth stations due to its simplicity and reliability and various types of directive feed horns have replaced the dipole feed except for some lower frequency applications. Reflector antennas can be grouped into:

1. Prime focus reflectors [9]
2. Offset reflectors [9]
3. Dual reflectors [9]
    - Splash plate [8]
    - Hat [10, 11]
    - Cassegrainian [12]
    - Gregorian [12]
    - Displaced axis [13]

The prime focus reflector is the most basic antenna configuration and the advantages being simplicity in manufacturing and pointing. On the negative side the blockage from the feed and support struts will cause diffraction and scattering which affects the radiation patterns and reflection coefficient.

The obvious advantage with the offset configuration is that blockage and scattering from the feed and struts are excluded. On the down side the radiation patterns will not be symmetrical and pointing and target tracking will become somewhat more complicated. The Green Bank radio telescope is the worlds largest steerable radio telescope and a grand example of an offset reflector antenna, Figure 2.1.

Figure 2.1: Large offset reflector antenna (The Green Bank telescope in West Virginia). Image courtesy of NRAO/AUI [14].

Dual reflector antennas offer an additional degree of freedom in the secondary reflector. These group of antennas may be of offset- or center fed configuration such as the hat feed which differs from traditional dual reflectors which were originally designed through ray tracing methods in the optical region. The hat feed operates through mode coupling in the near field region and this is examined in Chapter 4. The secondary reflector will cause blockage if center fed so classical dual reflector antennas are only competitive for antennas that is large in terms of wavelengths (typically $\geq 50\lambda$). The near field mode coupling of the hat feed allows a very small hat diameter (typically $\sim 2\lambda$) [6].

2.2 Antennas Feeds

The most common way to feed a reflector antenna is by using a corrugated horn [15]. This is a rather compact feed that generate nearly equal E- and H-plane radiation patterns with low cross polarization as a result. Wideband designs of 1.5:1 or more has been developed. For narrow flare angle feeds the directivity of the feed can be high, e.g. for dual reflector systems, but there will be frequency dispersion i.e. the phase center position of the feed will change with frequency. Examples of wideband feeds are:

- Quad ridge horn [15]
- Vivaldi antenna [16]
- Log periodic horns [17]

The Eleven antenna [18] developed at Chalmers is an example of a log periodic horn and its wideband performance and stable phase center makes it a suitable feed for radio astronomy [19, 20, 21]. Other feed types to mention are hard horns [22] which can be made compact and dipole feeds [16] for lower frequencies.

2.2.1 The Rear Radiating Cutler Feed

A pioneer in the design of reflector antennas and feeds for microwaves was C. C. Cutler from Bell Laboratories. An excellent introduction for the understanding of reflector antennas and practical design considerations was published in 1947 [8]. A simple reflector feed is achieved by placing a dipole antenna in the focal point of a reflector and adding a reflecting plane sheet, half cylinder or hemisphere at an appropriate distance for constructive phase contribution and illumination of the main reflector. The subtended half angle from the feed is normally $\leq 70^\circ$ for proper illumination and reduced cross polarization. However, differences in E- and H-plane radiation from this type of feed limits its applicability.

In an early attempt of a self supported rear radiating feed a metallic disk was placed in front of a circular waveguide going through the center of the parabolic reflector [8]. The radiation patterns did deviate from expectation and first at a later stage it was found that the radiation from the feed is not spherical but toroidal with a phase center in the form of a ring laying between the waveguide- and disk edge. The term ring focus feed was born and the associated reflector shape should be that of a parabola rotated around the focus ring i.e. being displaced by the ring focus radius. The radiation

characteristics can be improved by introducing a ring under the disk or replacing the disk by a cup. In the ring focus feed the TE_{11} and TE_{12} modes are excited and this combination causing almost straight field lines from the feed aperture plane with controlled illumination in the E- and H-planes as a result. The limiting factor is the impedance matching.

2.2.2 Dual Mode Horn

Dual mode horns can be used for obtaining a uniform illumination of a reflector with steep edge taper [15]. For a rectangular variant the TE_{10} and TE_{30} are excited by introducing a step causing a discontinuity. With proper amplitude and relative phase of these two modes the resulting aperture distribution results in the desired conditions for uniform amplitude and phase. This step will also excite the TE_{20} mode but if symmetry is maintained in the central plane this mode will not propagate. A serious limitation of the dual mode horn in many applications is its limited bandwidth.

2.3 Array Antennas

Array antennas [16] are popular in specialized applications due to their low profile and ability to scan the beam. Multiple antennas are grouped to yield highly directive patterns by adding the field constructively in the required directions and destructively elsewhere. Beam scanning is achieved by varying the phase excitation currents of the antenna array elements. Furthermore, the amplitude of the excitation currents can be varied to produce a wide range of radiation patterns with different sidelobe characteristics. However, the technology is costly and the losses in the feed network is high. Also the presence of grating lobes during beam scanning is a restriction for satellite communications with stringent sidelobe requirements. However, with reduced component costs and advances in the array development this technology is of interest not the least in airborne, train and automotive applications. An example of a phased array antenna is the 3D multi-role radar antenna, Figure 2.2.

2.4 Earth Station Minimum Technical and Operational Requirements

Earth terminals in transmit mode (Tx) must comply with certain criteria not to interfere with neighboring satellites and these requirements are also recom-

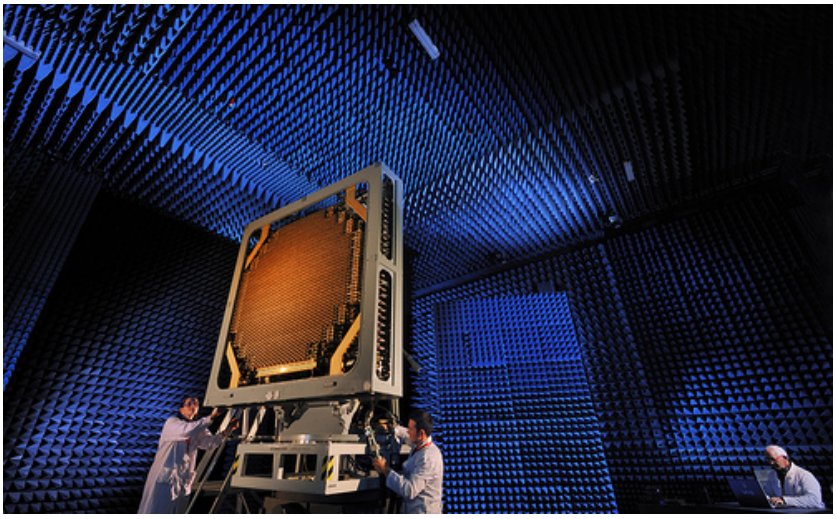

Figure 2.2: Phased array antenna under test (The MFRA C-band naval radar). Image courtesy of Finmeccanica [23].

mendations in receive mode (Rx). The sidelobe levels in the Tx-Ku-Satellite-band (13.75-14.50 GHz) are required below certain sidelobe envelopes to be certified by the European Telecommunications Standards Institute, ETSI [24]

$$\begin{array}{rlll} 29 - 25log_{10}\theta & dBi & for & \alpha < \theta \leq 7^{\circ}, \\ +8 & dBi & for & 7 < \theta \leq 9.2^{\circ}, \\ 32 - 25log_{10}\theta & dBi & for & 9.2 < \theta \leq 48^{\circ}, \\ -10 & dBi & for & 48 < \theta^{\circ}. \end{array} \tag{2.1}$$

For linear polarization the cross-polar sidelobe envelopes in the Tx-band as specified by the ETSI are

$$\begin{array}{rlll} 19 - 25log_{10}\theta & dBi & for & 1.8 < \theta \leq 7^{\circ}, \\ -2 & dBi & for & 7 < \theta \leq 9.2^{\circ}, \end{array} \tag{2.2}$$

where θ is the angle, in degrees, between the main beam axis and any direction towards the geostationary satellite orbit and within the bounds between 3° North and 3° South of the geostationary satellite orbit (as seen from the center of the earth). For antennas with a D/λ ratio $\leq$30, over the full extent of the antenna transmit frequency bands, the gain of the antenna sidelobe peaks should not exceed

$$\begin{array}{rlll} 32 - 25log_{10}\theta & dBi & for & \alpha < \theta \leq 48^{\circ}, \\ -10 & dBi & for & 48 < \theta^{\circ}. \end{array} \tag{2.3}$$

The angle α equals 100λ/D or 1° whichever is greater. In case of non circular antenna apertures D is the dimension in the plane of the geostationary orbit. Over the full extent of the antennas Tx-bands, no more than 10% of the antenna sidelobe peaks shall exceed the envelopes specified. Any individual peak shall not exceed those envelopes by more than 6 dB when $\theta > 9.2°$ and by more than 3 dB when $\theta \leq 9.2°$. Over the full extent of the antenna Tx-bands, the antenna polarization discrimination in the direction of the satellite shall be ≥35 dB everywhere within a cone centered on the main beam axis, with the cone angle defined by the pointing error or the -1 dB contour of the main beam axis, whichever is greater. This is also the recommendation for the Rx-band. Earth stations may operate with a polarization discrimination down to 25 dB, provided that the power density of the transmitted carrier does not exceed 34 dBW/4kHz. The maximum allowed EIRP (Effective Isotropic Radiated Power) is given for a G/T equal to 0 dB/K (for a specific location, the satellite G/T given needs to be subtracted from the specified EIRP value). To protect from transmissions on neighboring satellites, the antenna main beam axis shall not deviate by more than ±0.4° from the nominal direction of the satellite along the geostationary orbit, at all wind speeds at which the earth station may have to operate. The off-axis EIRP in any 40 kHz band in the direction of an adjacent satellite shall not exceed the following values

$$\begin{array}{lllll} 31 - 25log_{10}\theta & dBW & for & \alpha < \theta \leq 7°, \\ +10 & dBW & for & 7 < \theta \leq 9.2°, \\ 34 - 25log_{10}\theta & dBW & for & 9.2 < \theta \leq 48°, \\ -8 & dBW & for & 48 < \theta°. \end{array} \tag{2.4}$$

The orthogonally polarized component of the off-axis EIRP in any 40 kHz band should not exceed

$$\begin{array}{lllll} 21 - 25log_{10}\theta & dBW & for & 1.8 < \theta \leq 7°, \\ +0 & dBW & for & 7 < \theta \leq 9.2°. \end{array} \tag{2.5}$$

In recent years many Ultra Small Aperture Terminals (USAT) have been developed especially for satcom on the move applications for trains, buses, ships & aircrafts etc where small antenna size is a requirement. The USAT size may have a D/λ ratio of ≤30. As the original ETSI regulations evolved with large stationary earth stations in mind there have been a complementary standard for USAT namely the Standard M-x [25]. This certification can be given to USAT's not fulfilling the ETSI requirements on co- and cross polarization but meets all other regulations. The certification is initially

given for a 6 month period in association with a valid transmission plan. The conditions are:

- A minimum transmit cross-polar discrimination of 20 dB within the -1 dB contour of the main beam
- A maximum allowed EIRP density in compliance with the off-axis emissions constraints from (2.4)
- Antenna diameter $\leq$2.4 m

The co- and cross-polar sidelobe masks described are plotted in Figure 2.3.

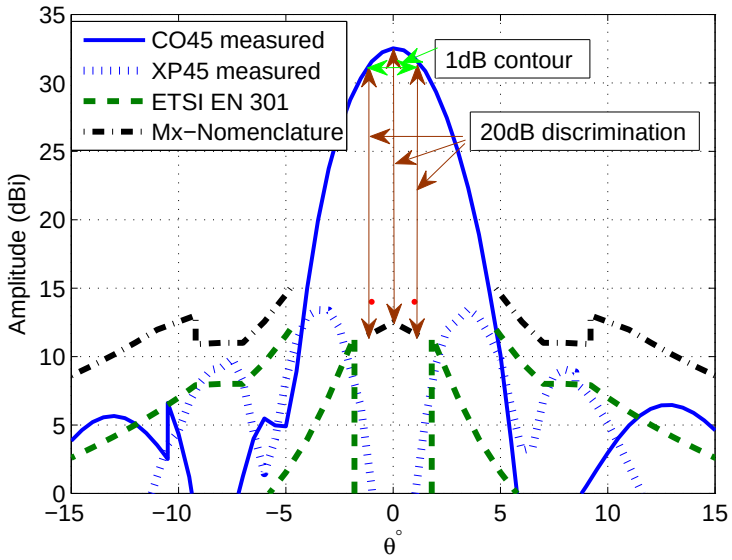

Figure 2.3: Co- and cross-polar sidelobe envelopes including the 20 dB cross-polar discrimination requirement within a 1 dB contour of the main beam. Example antenna radiation patterns are included.

Chapter 3

QuickWave-V2D & Genetic Algorithm for Simulation and Optimization

3.1 QuickWave-V2D

When simulating the hat-fed reflector antenna; computational time and accuracy in the modeling are the two most important aspects when selecting an EM simulation software. As the hat-fed reflector antenna is axisymmetrical and a body of revolution (BOR) [26] it is possible to use a 2D simulation tool and considerably reduce simulation time compared to 3D modeling.

QuickWave-V2D (QW-V2D) utilizes the conformal FDTD method in a vector two-dimensional (V2D) formulation, expressed in cylindrical coordinates [27]. It incorporates models for curved boundaries, media interfaces, modal excitation, and parameter extraction. This V2D electromagnetic solver is applicable to the analysis of BOR-structures as large as 300λ. The simulation time can be reduced by a factor 100 or more compared to brute force 3D analysis. It was proven in [28] that structures maintaining axial symmetry of boundary conditions belong to a class of V2D problems. The total electromagnetic field in such structures can be decomposed into a series of orthogonal modes, of different angular field dependence of the $\cos(n\phi)$ or $\sin(n\phi)$ type, where ϕ is an angular variable of the cylindrical coordinate system and n=0,1,2.. Each n-mode is analyzed separately in QW-V2D. Based on this the numerical analysis can be done in 2D, over one half of the symmetrical structure, with n predefined as a parameter. The n-mode must not be confused with waveguide modes e.g. a QW-V2D analysis with n=1 takes into account a composition of all circular waveguide modes TE_{1k} and TM_{1m} where k and m are arbitrary natural numbers.

3.2 Optimization Methods Overview

Optimization is a requirement in most systems and applications and it has found steady increased interest in electromagnetic problems in recent years.

There are many optimization methods that can be applied e.g.:

- Genetic Algorithm [29]
- Particle swarm [30]
- Differential evolution [30]
- Hill climbing [31]
- Quasi-Newtonian [31]
- Simulated annealing [31]
- Random walk [32]
- Conjugate gradient [32]
- Monte Carlo [32]

The optimization methods can be grouped into the two main categories: *Deterministic-* and *Stochastic* optimization methods [32]. *Deterministic* algorithms follow a rigorous procedure and its path and values of both design variables and functions are repeatable. Hill climbing is an example of a deterministic algorithm and it will give identical output in any re-optimization. An inherent property of a *stochastic* optimization, on the other hand, is that it include randomness. The genetic algorithm is an example and the string or solution in the population will be different for each optimization as the algorithm use pseudo random numbers and even if the end results may be very similar the path there is not exactly repeatable. There are also *hybrid* methods e.g. Hill climbing with random restart. The method to chose depends on the type of problem to solve e.g. the number of variables and complexity. Work has also been done with focus on fast optimization of a special electromagnetic problem [33, 34]. In this thesis we focus on the Genetic algorithm which is considered most suitable for finding the global optimum of the relatively complex optimization problem of the hat feed. The genetic algorithm have been successfully applied not only in electromagnetics but also other fields of engineering, computer science and finance [29].

3.3 Genetic Algorithm

The Genetic Algorithm (GA) is a stochastic search method based on the Darwinian principles of natural selection and evolution. The method is especially effective in finding global maximum in a high dimensional multimodal function domain in particular when the problem is cast in a combinatorial form [29]. In the GA a set or population of potential solutions is caused to evolve towards a global optimal solution. This is done by introducing a fitness weighted selection process and recombination and mutation of existing characteristics or parameters. Much of the GA terminology comes from nature [29]:

- Gene - optimization parameter
- Chromosome - string of genes (trial solution vector)
- Generation - successively created population
- Population - set of trial solutions
- Parent - member of current generation
- Child - member of next generation
- Fitness - number representing goodness of individual

The genes are the basic building blocks of the optimization and generally a coded representation of individual optimization parameters. The genes are grouped in chromosomes which may be coded as a binary string, real numbers or a combination of the two. When decoded the chromosome represents a trial solution. A set of chromosomes constitutes a population which is utilized by the GA to find the optimum solution. In the GA optimization each iteration is called a generation. The procedure in each iteration is selection combining and mutating until the new, and preferably fitter, generation is formed. The idea is that highly fit individuals, i.e. highly fit characteristics, reproduce resulting in a drift in subsequent generations towards an optimum solution. The optimization can be terminated when a threshold value on the characteristics is reached or when a specific number of iterations is made.

In the initialization process a population is generated randomly within certain defined limits. Pairs of individuals, the parents, are selected in a probabilistic manner weighted by their relative fitness. The weighted roulette wheel is a typical scheme where each individual is assigned a space on the

roulette wheel proportional to the fitness value. Each time a parent is required the wheel is spun and the fitter individuals are more likely to be chosen due to their larger space on the roulette wheel.

The offspring, or children, are generated from the selected pair of parents through simple stochastic operators crossover and mutations. Crossover is a random recombination of two parents and typically occur with a probability 0.6-0.8. Recombination and selection is the basic principle of GA evolution. Mutation which typically occur with a low probability (e.g. 0.05) hinder premature convergence and help exploring new regions by introducing random valued genes.

Each individual is assigned a fitness value related to the fitness function or optimization goal. The fitness function is the link between the GA optimization process and the physical problem.

The GA is a global optimization method which means that the result should be independent of starting point in contrary to local optimization techniques. Global techniques are much better at dealing with solution spaces having discontinuities, constrained parameters, and or a large number of dimensions with many potential local minima [29]. The downside is that the local solution space is not taken advantage of leading to a slower convergence compared to local techniques.

Chapter 4

The Hat Feed

4.1 Basic Concept of the Hat Feed

The hat feed was first presented in 1986 by Kildal [35] as a self supporting feed with low cross polarization (30 dB) and no blockage or scattering from support struts. A limitation was the narrow bandwidth of the reflection coefficient. A characteristics of the hat feed is that the feed waveguide contributes to the radiation in a controlled and favorable way unlike other self supported feed technologies. The feed consists of a circular waveguide (the neck), a dielectric spacing (the head) and a corrugated disk (the hat), Figure 4.1. The fundamental TE_{11} mode is propagating in the waveguide and couples to two different modes in the radial direction namely the the $\phi-$ mode with E$-$ field in the $\phi-$ and $\rho-$ direction and the z$-$mode with E$-$field only in the z$-$direction. The $\phi-$mode radiates only in the H$-$plane and not along the neck. The z-mode radiates mainly in the E$-$plane and also strongly along the neck in both the E$-$ and H$-$planes. The two modes can be denoted E$-$ and H$-$plane modes respectively [10]. By exciting the two modes with correct phase and amplitude it is possible to obtain equal E$-$ and H$-$plane patterns and thereby low cross polarization. The corrugations of the hat brim is traditionally $\lambda/4$ deep causing the normal z$-$component of the E$-$field to be zero along the brim. The corrugated brim is therefore a soft surface as defined in [36] and results in increased symmetry of radiation patterns, reduced cross polarization and spillover sidelobes. It is possible to replace the dielectric head with metal rods for a robust and low cost solution but this results in reduced beam symmetry [37].

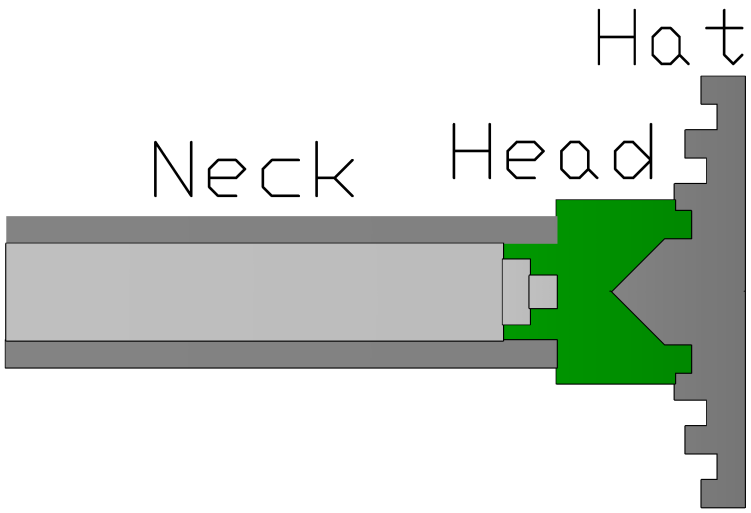

Figure 4.1: Profile of the hat feed with its three main parts.

4.2 Ring Focus

Conventional feeds can be seen as a point source generating spherical waves. Maximum efficiency is obtained when the phase center of the feed coincides with the focal point of the reflector. The hat feed, on the other hand, has a ring shaped phase center generating an elliptical wave [38]. As a result the reflector should be of ring focus type for minimized phase error and optimum efficiency. The hat feed radiates from a circumferential aperture rather than a planar field in free space so the radiation field is best characterized as ring shaped phase center rather than a phase center point. The optimum reflector shape for such ring focus feed is the ring focus paraboloid. The formula for the shape of the ring focus paraboloid [38]

$$\rho = 2F\tan(\theta_f/2) + \rho_{R0}, \quad z = F - F\tan^2(\theta_f/2), \tag{4.1}$$

with ρ_{R0} being the radius of the reflectors focus ring, F the focal length and and θ_f the polar angle of the feed as defined in Figure 4.2. The ring focus radius, ρ_{R0}, can be determined by calculating the phase of the radiation field function of the feed or from the phase of the aperture field. The difference in reflector shape can be up to 0.25λ for deep reflectors and less for shallow ones. By using a ring focus reflector the aperture efficiency may be up to 1 dB better than if a paraboloidal reflector is used [39].

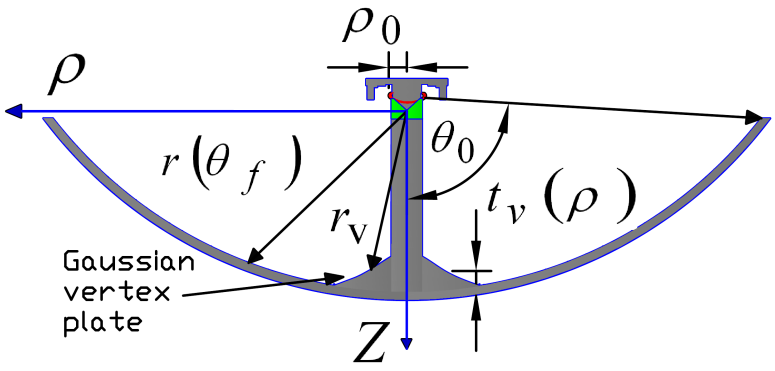

Figure 4.2: Hat-fed reflector antenna with Gaussian vertex plate.

4.3 Gaussian Vertex Plate

Multiple reflections between reflector and feed may have a critical effect on the reflection coefficient and the radiation patterns. By introducing a flat vertex plate at the center of the reflector the multiple reflections can be reduced and the reflection coefficient improved. Positive effects have also been seen in terms of reduction of sidelobe levels and increased directivity due to reduced center blockage and multiple reflections between reflector and feed as investigated in [40]. The contribution of multiple reflections and its influence on G/T was analyzed further in [41] using the method of moments (MoM). The evolution of vertex plates eventually lead to a Gaussian shape for improved performance [42]. The Gaussian vertex plate can make the reflected field from the reflector a null at the focus of the reflector where its feed is located, and this therefore minimizes the degrading effect of the multiple reflections and reduces the diffractions from the brim of the hat. In addition to this, the Gaussian vertex plate reduces far-out sidelobes. The derivations lead to the following design formulas for the shape of the Gaussian vertex plate [42]

$$t = t_0 e^{-(\rho/\rho_0)^2}, \tag{4.2}$$

with

$$t_0 = 0.15\lambda, \qquad \rho_0 = 0.5\sqrt{(F\lambda)}, \tag{4.3}$$

where λ is the wavelength at the design frequency. The Gaussian vertex plate parameters are shown in Figure 4.2.

4.4 Antenna Noise Temperature and G/T

Antennas pick up noise from the sky and the warm ground. Additionally feed cables and the LNA (Low Noise Amplifier) are also contributors to the noise level. The noise level depends on the elevation angle of the antenna and the radiation patterns. High spillover sidelobes will pick up noise from the warm earth and critically reduce G/T (Gain over Antenna Noise Temperature). The noise from the ground is not constant but depends on the type of soil, roughness and polarization of the antenna. A computer program for calculating G/T of an antenna with known co- and cross-polar radiation patterns in the 45° plane using MoM and MR (Multiple Reflections) techniques was developed in [43]. Furthermore, ohmic losses in the feed line and noise figure of the LNA can be included in the analysis if known. Typical numbers of brightness temperature is 2.7 K, 80 K, and 293 K for 90°, 0° and -90° elevation respectively. The system noise temperature can be described as [43]

$$T_{sys} = T_c + T_{rec} + T_{ant}, \tag{4.4}$$

where T_c is the noise contribution from the cable loss

$$T_c = T_0(1 - \eta_c)/\eta_c, \tag{4.5}$$

with the transmission efficiency

$$\eta_c = 10^{-L_{dB}/10}. \tag{4.6}$$

A LNA with noise factor NF_{dB} results in the following noise temperature at the terminal [43]

$$T_{rec} = 293K10^{NF_{dB}/10-1}/\eta_c. \tag{4.7}$$

4.5 Characterization of the Hat Feed

4.5.1 Efficiency

The efficiency is an important parameter in the characterization of antennas. The maximum available directivity from an aperture is [9]

$$D_{max} = \frac{4\pi}{\lambda^2}A, \tag{4.8}$$

with A being a plane aperture area.

The efficiency of a feed, the feed efficiency, can be separated into sub-efficiencies representing spillover-, cross polarization-, illumination- and phase error loss. The term feed efficiency was introduced and factorized by Ludwig in [44] and later further analytically formulated for reflector feeds by Kildal [45]. The expressions in [45] is for the 45° plane of the co- and cross-polar radiation fields rather than for the E- and H-planes. We find that the co-polar patterns are the mean of the E- and H-plane patterns and that the cross-polar patterns are the half difference between the E- and H-plane patterns. The feed efficiency can be factorized into [9]

$$e_{ap} = e_{BOR1} e_{sp} e_{pol} e_{ill} e_{phi}. \tag{4.9}$$

The term e_{BOR1} is the BOR_1 (Body of Revolution) efficiency as derived in [26]

$$e_{BOR_1} = \frac{\pi \int_0^{\pi} [|A_1(\theta)|^2 + |C_1(\theta)|^2] sin\theta d\theta}{\int_0^{\pi} \int_0^{2\pi} |I_y(\theta,\varphi)|^2 (cos^2\theta sin^2\varphi + cos^2\varphi) sin\theta d\theta d\varphi}. \tag{4.10}$$

The nominator is the power in the first order φ-modes and the denominator is the total power radiated by a dipole in free space. The terms $A_1(\theta)$ and $C_1(\theta)$ are the E- and H-plane radiation field functions respectively. Since the hat feed is a BOR_1 antenna this sub-efficiency is unity.

The spillover efficiency e_{sp} is the power within the subtended angle θ_0 (i.e. the power hitting the reflector) relative to the total power radiated by the feed, Figure 4.3. The equation is given as [9]

$$e_{sp} = \frac{2\pi \int_0^{\theta_0} [|G_{co45}(\theta_f)|^2 + |G_{xp45}(\theta_f)|^2] sin\theta_f d\theta_f}{2\pi \int_0^{\pi} [|G_{co45}(\theta_f)|^2 + |G_{xp45}(\theta_f)|^2] sin\theta_f d\theta_f}. \tag{4.11}$$

The illumination efficiency e_{ill} is a measure on how well the power from the feed is distributed over the reflector, as illustrated in Figure 4.3, and the equation is given by [9]

$$e_{ill} = 2cot^2(\frac{\theta_0}{2}) \frac{[\int_0^{\theta_0} |G_{co45}(\theta_f)| tan(\frac{\theta_f}{2}) d\theta_f]^2}{\int_0^{\theta_0} |G_{co45}(\theta_f)|^2 + sin\theta_f d\theta_f}. \tag{4.12}$$

The polarization efficiency e_{pol} is the co-polar power over the total radiated power both within the subtended angle θ_0. The equation is given as [9]

$$e_{pol} = \frac{\int_0^{\theta_0} |G_{co45}(\theta_f)|^2 sin\theta_f d\theta_f}{\int_0^{\theta_0} [|G_{co45}(\theta_f)|^2 + |G_{xp45}(\theta_f)|^2] sin\theta_f d\theta_f}. \tag{4.13}$$

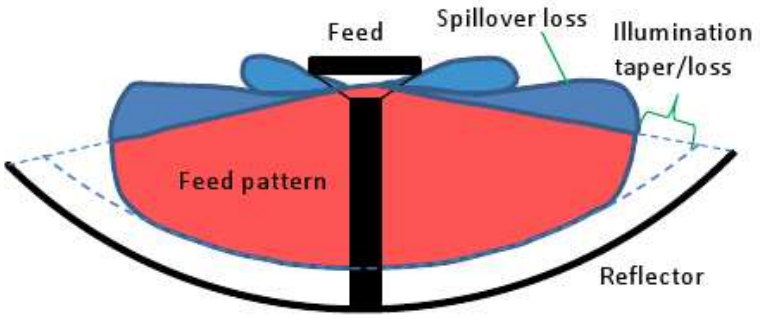

Figure 4.3: Radiated field from feed to reflector with spillover- and illumination loss highlighted.

Finally the phase efficiency is given by [9]

$$e_\phi = \frac{|\int_0^{\theta_0} G_{co45}(\theta_f)|tan(\frac{\theta_f}{2})d\theta_f|^2}{[\int_0^{\theta_0} |G_{co45}(\theta_f)|tan(\frac{\theta_f}{2})d\theta_f]^2}. \tag{4.14}$$

This sub-efficiency is depending on the phase center of the feed relative to the focal point of the reflector. For the hat feed the phase efficiency can approach unity by using a reflector of ring focus type, see section 4.2, instead of a conventional paraboloid which would reduce the phase efficiency.

4.5.2 Co- and Cross-Polar Radiation Patterns

The co- and cross-polar radiation patterns of a BOR_1 antenna can be written as [26]

$$G_{CO}(\theta, \varphi) = G_{co45}(\theta) - G_{xp45}(\theta)cos(2\varphi), \tag{4.15}$$

$$G_{XP}(\theta, \varphi) = G_{xp45}(\theta)sin(2\varphi). \tag{4.16}$$

This states that the radiation characterization of a BOR_1 antenna is determined by only the co- and cross-polar radiation functions in $\varphi = 45°$ plane, i.e., $G_{co45}(\theta)$ and $G_{xp45}(\theta)$.

4.5.3 Reflection Coefficient

The reflection coefficient Γ is the ratio of the amplitude of the reflected wave to the amplitude of the incident wave. For the hat-fed reflector antenna Γ

is defined at the input port of the circular waveguide when the hat feed illuminates the reflector. Γ can be expressed in terms of complex radiation impedance $Z_a = R_a + jX_a$ and the characteristic impedance of the transmission line $Z_c = R_c + jX_c$ as [9]

$$\Gamma = \frac{Z_a - Z_c}{Z_a + Z_c}. \tag{4.17}$$

Chapter 5

Radome

5.1 Background

The term radome comes from *rad*ar d*ome* and is a cover enclosing the antenna to protect from rain, ice, wind, UV light, dust and other environmental influences. The requirements are both mechanical and electrical. The radome must be rigid enough to manage vibrations of various resonance frequencies, extreme wind gusts and mechanical loads from collisions (most stringent for aircraft radomes). The radome should also affect the electrical antenna performance as little as possible i.e. parameters such as reflection coefficient, co- and cross-polar radiation patterns should remain essentially unaffected. Radomes can be of arbitrary shape depending on antenna and application but planar-, conical-, and spherical form dominates. For large radome sizes where tool sizes and transportation becomes impractical, e.g. for radio telescopes, the radome can be constructed from several panels joined together. The panels can be joined by metallic fixings but this will degrade the radiation patterns. The radome is preferably covered with a hydrophobic coating to minimize the attenuation effects of water on the surface. The coating may be a variant of silicon or Polytetraflouraethylene also known as Teflon®. Some useful electrical material properties of radome materials are shown in Table 5.1.

It was during the introduction of aircraft fighter radars in World War II that the need for radomes arose and an early example is the hemispherical nose cone plexiglass radome protecting an Western Electrical S-band radar on a B-18A aircraft in 1941 [46]. Plywood was early evaluated as radome material but due to moist uptake and difficulties in the shaping it was abounded. More successfully a three layer sandwich with fiberglass skins and polystyrene fiber core was developed by MIT Radiation Laboratory in

1944 and this became the current state of the art [46]. Since World War II the antenna materials have developed into the main categories of ceramics for hyper velocity missile radomes and high strength organic materials for composite radomes. In this work we will not discuss ceramics but focus on organic monolayer- and sandwich structures. An example of a radome enclosing a reflector antenna is shown in Figure 5.1.

Figure 5.1: Example of radome enclosing reflector antenna (cut open for visualization). Image courtesy of Skycom Telecom [47].

5.2 Monolayer Radome

The most basic radome type is the monolayer structure. Low loss organic plastic materials such as HIPS (High Impact Poly-Styrene) or Polycarbonate is often used. This type of radome is preferably chosen for small or medium size radomes with moderate requirements on mechanical strength and electrical bandwidth. It is easily serial produced through a vacuum forming process using a moulding tool. The radome thickness (t) is normally chosen with

$$t = n * \lambda/2\sqrt{(\epsilon)} \text{ with n=1,3,5,...} \tag{5.1}$$

A manufactured monolayer radome under test of reflection coefficient is shown in Figure 5.2.

Figure 5.2: Monolayer radome under test. Manufactured by Arkivator AB.

5.3 Sandwich Radome

When good mechanical strength and low weight is required the sandwich radome is an attractive configuration. The sandwich consists of two skins separated by a lightweight core. The skins may be a mixture of e-glass and epoxy while the core being a polyurethane foam or honeycomb structure. The skins are made as thin as mechanically feasible and with a core spacing (s) of

$$s = n * \lambda/4\sqrt{(\epsilon)} \text{ with n=1,3,5,...} \tag{5.2}$$

A manufactured sandwich radome prototype for satellite earth station is shown in Figure 5.3.

5.4 Radome Effects on Antenna Performance

5.4.1 Boresight Error

Boresight Error (BSE) is an angular deviation of the main beam from boresight after introduction of the radome [46]. This is due to a distortion of the electromagnetic wavefront through the dielectric material. The BSE is

Figure 5.3: Sandwich radome with access hatch for satellite earth station. Manufactured by Art&Technology.

depending on frequency, polarization and antenna orientation and the BSE is an important factor when determining the required manufacturing tolerances.

5.4.2 Sidelobe Degradation

The antenna sidelobes generally increase or shift slightly when introducing the radome due to distortion and transmission effects. For some low sidelobe antennas the radome may be the major source of sidelobes.

5.4.3 Depolarization

Depolarization indicates that energy is transferred from the co-polarized to the cross-polarized component e.g. from RHCP to LHCP or vice versa. This is en effect from the radome curvature and the difference in complex transmission coefficient between orthogonal polarized vectors. This is problematic for satellite earth stations utilizing frequency reuse i.e. transmitting

or receiving two independent signals with the same frequency but orthogonal polarizations [46].

5.4.4 Voltage Standing Wave Ratio

The radome may have a critical influence on the antenna Voltage Standing Wave Ratio (VSWR). Part of the electromagnetic wave is reflected at the radome layers which reduce the antenna gain.

5.4.5 Insertion Loss

The radome insertion loss is a result of the attenuation of the electromagnetic wave when propagating through the radome material. This loss is due to the reflection at the radome interfaces and dissipation in the dielectrics which is a function of the material loss tangent, $tan\delta$ [46].

5.5 Advances in Radome Development

5.5.1 Metamaterials

Metamaterials is a relatively new science and the word was coined in 1999 by R. Walser at the University of Texas who defined it as "microscopic composites having a man made three-dimensional periodic cellular architecture designed to produce an optimized combination not available in nature" [48]. It may result in a negative index and refraction and a reversal of Snells law. Using metamaterials in radomes has been reported to increase directivity and gain of antennas [49]. By combining one layer of negative valued refractive index material with one positive valued layer it was shown possible to eliminate refraction.

5.5.2 Frequency Selective Surfaces

There are various scenarios where Frequency Selective Surfaces (FSS) on a radome would be applicable. On board ships for example a FSS would protect the satellite earth station from scanning high power radars. A FSS can take many forms and strips, slots, square loops and Jerusalem crosses have all been used in array configuration on the radome surface [46]. These antenna elements that are normally etched on the radome will either transmit or reflect electromagnetic waves with wavelengths related to the array elements.

Table 5.1: Radome material properties at 10 GHz.

Material	Permittivity (ϵ)	Loss tangent (δ)
Polycarbonate	2.9	0.005
HIPS	2.55	0.00033
E-glass	6.06	0.004
Epoxy	4.4	0.016
Polyurethane foam	1.05	0.0005

Chapter 6

Optimization and Measurement of Hat-Fed Reflector Antenna with Radome

In this chapter we will apply the theory and concepts from previous chapters and give a summary of the development work done towards this licenciate degree.

6.1 Optimization

In the GA optimization the hat feed geometry is described by a chromosome which includes all 24 dimensions of the hat feed, Figure 6.1.

Several of the parameters have been set to fixed values through the optimization. The waveguide inner radius (R) is set to the standard value 9 mm to match the waveguide interface of the OMT (Ortho-Mode Transducer). The waveguide wall thickness (T) is set to 1 mm. The hat brim radius which is the sum of w1+w2+..w7 is set to 29 mm which was chosen empirically by simulations. If this dimension was not fixed the radius would likely be too large and cause blockage when feeding a reflector. The subtended half angle was chosen empirically to $\theta_0 = 89°$ which corresponds to F/D=0.255 with F being the focal length (F=130 mm) and D the antenna diameter (D=530 mm). The aperture efficiency was simulated as a function of F/D-ratio and we see that for the chosen F/D-ratio the aperture efficiencies are $\geq$-1.2 dB and $\geq$-2.6 dB for the Tx- and Rx-band respectively, Figure 6.2.

The dielectric material for the head, Figure 4.1, to support the hat on top of the neck is Rexolite with ϵ_r=2.53 and tanδ=0.0001 at 10 GHz. The

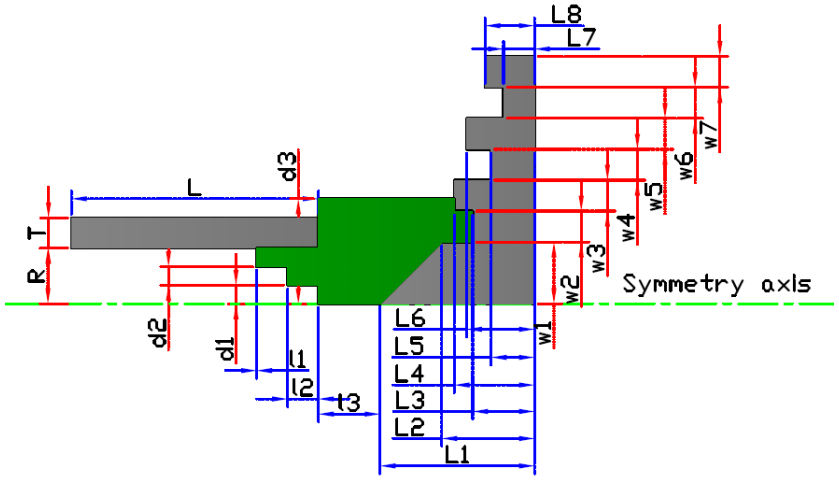

Figure 6.1: The parameters of the hat feed in the optimization.

optimization is multi objective and we optimize towards minimized reflection coefficient and maximized feed efficiency. Additionally we want the spillover efficiency to be ≥ -0.5 dB resulting in low G/T factor by minimizing the contribution on antenna noise temperature from the warm ground by spillover sidelobes. In the optimization we randomly generate an initial population of 500 individuals in order to have a good spread of genes. Then, each individual is simulated by QW-V2D and evaluated by its fitness value, Figure 6.4, using the developed GA code through Matlab for determining the likeliness for the individual to pass its genes to the next generation. A flow chart of the GA that was implemented and used in this work is shown in Figure 6.3.

Two individuals are selected as parents to produce two children in a crossover scheme. Mutation, a random change of a few genes, is used in this GA scheme to avoid local minima. The crossover probability is set to 80% and the mutation rate to 6%. The hat feed is modeled using QW-V2D utilizing approximately 11 000 mesh cells, with a mesh size of 1 mm, which requires 1 MB RAM. It is sufficient with 10 000 iterations to reach convergence and this takes approximately 10 seconds on a dual core 2 GB RAM computer. Completing an optimization with 500 individuals over 40 generations requires about 56 hours simulation time. After evaluation of the pareto front with all the fitness values a number of optimization results, or geometries, are chosen for further evaluation and simulation with reflector antenna. The feed efficiency and reflection coefficient is given by the optimization but the final co- and cross-polar radiation patterns of the hat-fed reflector antenna comes from manual simulations. The profile of the chosen hat feed, with best overall

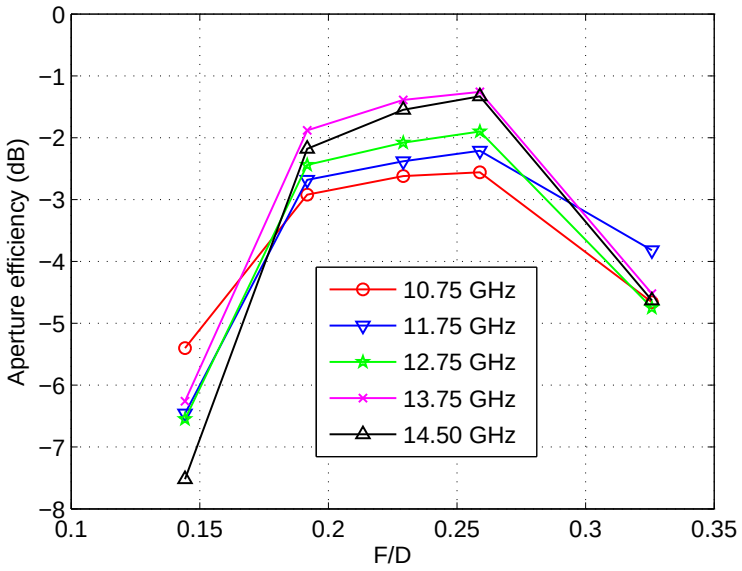

Figure 6.2: Simulated aperture efficiency of hat-fed reflector antenna as a function of F/D-ratio.

performance, is shown in Figure 6.5. The hat feed was manufactured from aluminium and dielectric Rexolite and a photo of the measured hardware prototype is shown in Figure 6.6.

6.1.1 Simulation Results

Hat Feed

The reflection coefficient of the hat feed was simulated and the results together with measurements are shown in Figure 6.7. We see that the reflection coefficient $\leq$-17 dB in both the Rx- and the Tx-band.

The radiation patterns of the feed are directly related to the e_{ill}, e_{spill} and e_{pol} optimization parameters. Strong illumination towards the vertex of the reflector will after reflection be blocked by the hat feed, or diffracted at the hat edge, so a dip of the radiated power in this central region is preferred. Apart from the center dip an even illumination of the reflector and steep taper at the reflector rim, $\theta = 89°$, is the ideal radiation from the hat feed. We see that there is a center dip in the radiation patterns for the Tx-band, Figure 6.8.

It is important to have control over the various sub-efficiencies and their frequency variations. We see that e_{pol} and e_{spill} is $\geq$-0.5 dB over the full band,

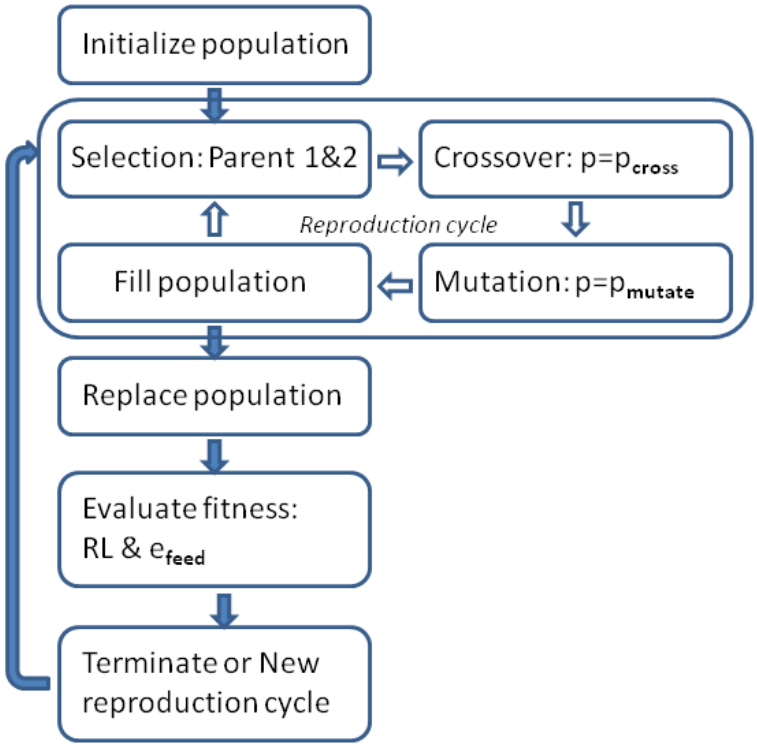

Figure 6.3: Flow chart of the implemented GA routine.

Figure 6.9, which indicate that the cross-polar sidelobe requirements can be met and that the G/T factor should be sufficiently high for the satellite earth terminal. The e_{ill} factor is contributing to the lower e_{opt} in the Rx-band and it can be seen in Figure 6.8 that the central part of the reflector is strongly illuminated and that the edge taper is $\geq 10\ dB$ resulting in illumination loss.

As discussed in chapter 4 the hat feed is of ring focus type and the ring focus radius was determined numerically. Figure 6.10 shows the phase efficiency of the optimized hat feed with different ring radii ρ_R and phase reference locations z. From this, we can obtain numerically that the optimal focal radius $\rho_{R0} = 6.8\ mm$ and the phase center $z_{pc} = 12\ mm$, with the origin of the coordinate system located at the peak of the cone of the hat. We see that the phase efficiency of the ring focus is approaching 0 dB.

The reflector diameter of 53 cm results in a compact satellite earth station with sufficient gain for the application, i.e. $\geq 33\ dBi$, based on the simulated efficiencies. The reflector is made from a 516.4 mm diameter paraboloid which is extended by a $2\rho_{R0} = 13.6\ mm$ diameter circle at the center.

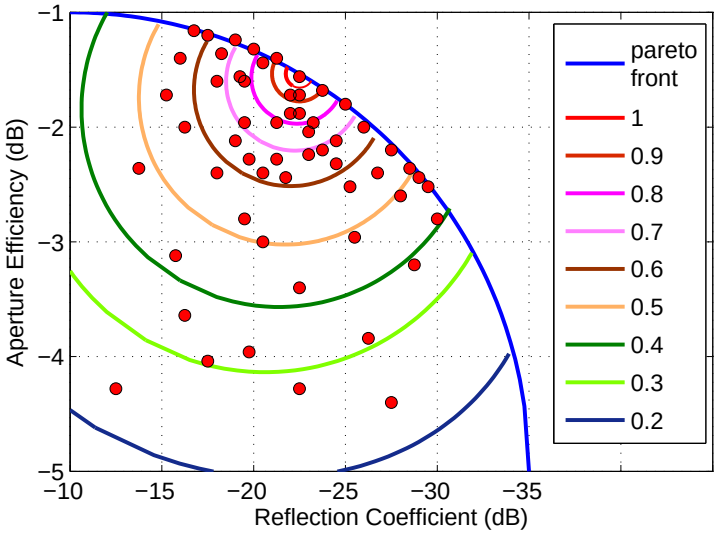

Figure 6.4: The pareto front with fitness values after hat optimization.

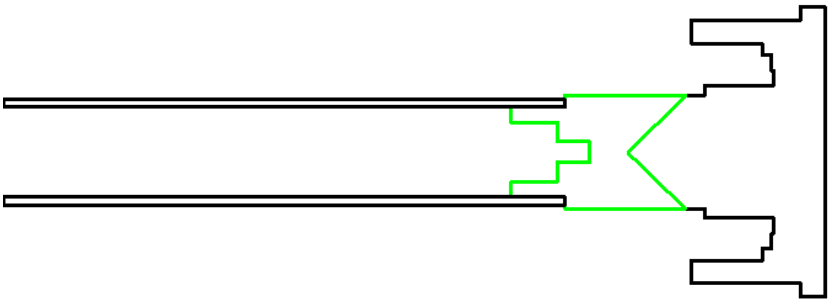

Figure 6.5: The profile of the optimized hat feed.

The efficiency of the hat feed and hat-fed reflector antenna using three different methods is presented in Figure 6.11. The legend *Simulated total feed efficiency* represent the sum of the calculated sub-efficiencies based on the simulated feed radiation function as defined by (4.9). The legends *Simulation of whole reflector* and *Measurement of whole reflector* is the ratio of the calculated directivity from the radiation patterns of the simulated and measured antenna over the theoretical maximum efficiency, (4.8), of a 53 cm circular aperture. We see that the agreement is very good.

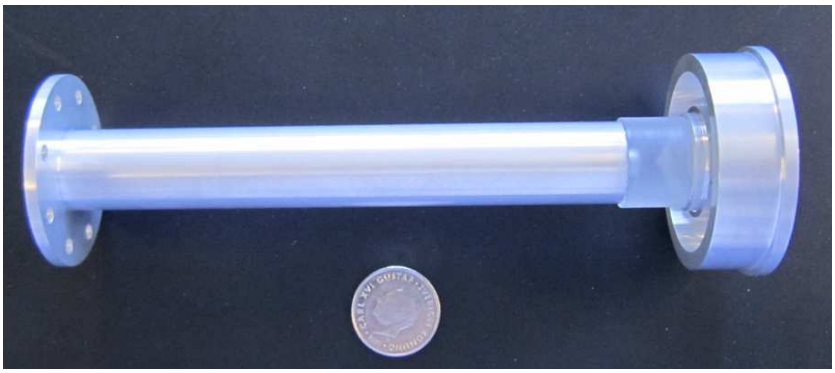

Figure 6.6: Photo of the optimized hat feed.

Gaussian Vertex Plate

A Gaussian vertex plate was implemented in order to reduce multiple reflections between reflector and feed. The design formulas in (4.2) and (4.3) are used with the design frequency 12.625 GHz or $\lambda = 23.76\ mm$ which results in $t_0 = 3.564\ mm$ and $\rho_0 = 27.788\ mm$, see Figure 4.2. The simulation and measurement results with and without Gaussian vertex plate are shown in Figure 6.12. It is clear from the simulation that the reflection coefficient show degraded performance, with periodic variations, in the absence of the Gaussian vertex plate due to multiple reflections between reflector and feed. This effect is strongest in the Rx-band where the radiated power along the waveguide towards the vertex is strong , Figure 6.8. In the Tx-band we find a dip in the field illuminating the vertex so the Gaussian vertex plate has less effect. The measurement was only done with Gaussian vertex plate in the center of the extended paraboloid and it shows low reflection coefficient $\leq -17dB$ and no periodic variations which is in line with the simulation results.

Radome

Based on the investigation in chapter 5 we chose to design a monolayer radome due to its simplicity in manufacture and seemingly satisfactory performance over the required bandwidth. The radome was simulated in QW-V2D by modeling a hemispherical radome in front of the optimized hat-fed reflector antenna, Figure 6.13. The material of the monolayer radome is polycarbonate with permittivity ($\epsilon = 2.9$) and loss tangent ($\delta = 0.005$), as found in Table 5.1. The simulated reflection coefficients of the hat-fed reflector antenna when enclosed by monolayer radome of various thickness is shown in, Figure 6.14. The least effect is found for the radome thickness 8 mm which

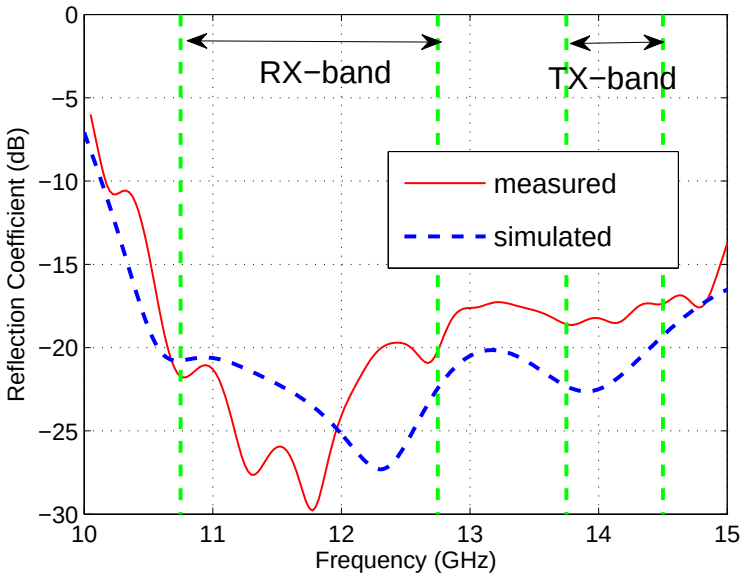

Figure 6.7: Reflection coefficient of hat feed. Simulation and measurement without reflector.

corresponds to $\lambda/2$ in the dielectric at 11 GHz. After manufacturing through vacuum forming it was found that the final thickness was measured to 7.14 mm which corresponds to $\lambda/2$ in the dielectric at 12.35 GHz.

6.2 Measurements

6.2.1 Hat-Fed Reflector

Measurements were done on a 53 cm ring focus reflector fed by the optimized hat feed. The F/D ratio of the reflector is 0.255 and the feed is placed with its ring focus phase center in the position of the reflectors focal distance of 130 mm. This means that the subtended half angle of the feed is $\theta_0 = 89°$ as in the hat feed optimization. The hat-fed reflector antenna under test is shown in, Figure 6.15. The co- and cross-polar radiation patterns are measured in the $\varphi = 45°$ plane and presented together with the sidelobe envelope masks of the ETSI (2.1) and (2.2) as well as M-x standards (2.3) in, Figure 6.16-6.20.

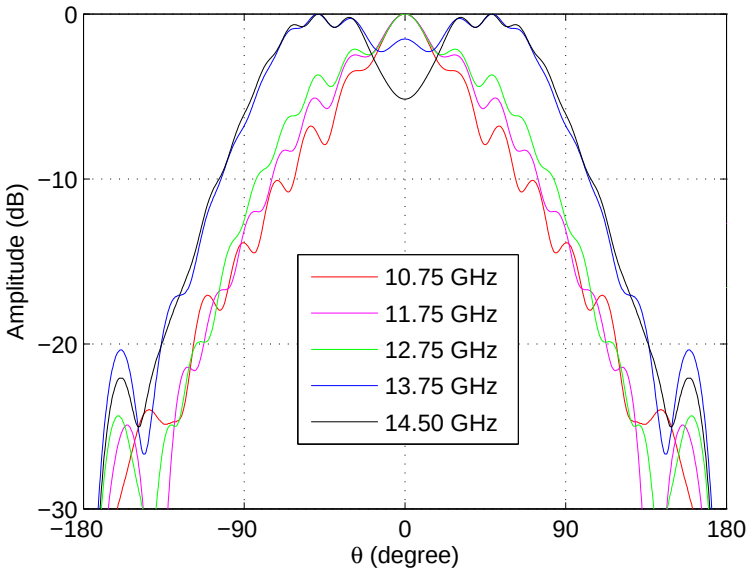

Figure 6.8: Simulated radiation patterns in the $\varphi = 45°$ plane of the hat feed.

6.2.2 Radome with Hat-Fed Reflector

The transmission coefficient of the radome is measured by placing two conical horns (55 mm long, 95 mm in diameter and fed by a 18 mm diameter circular waveguide) with the distance 7.14 mm. The transmission coefficient S_{21} is measured with and without the radome in between. The difference is plotted in, Figure 6.21.

In the Tx-band, the difference is only about 0.1 dB, indicating that the ohmic loss of the radome is $\leq$0.1 dB. In the Rx-band, due to the reflection of the radome, there may be a radiation leakage, so the difference is slightly bigger. However, the assumption is that the ohmic loss in the Rx-band is similar to that in the Tx-band. Measurement results of radiation patterns in the $\varphi = 45°$ plane identical to the setup of, Figure 6.16-6.20 but with coverage of the radome is shown in, Figure 6.22-6.24. The radome effect on the main lobe is hardly seen and the effect on the sidelobes is only minor i.e. the levels are similar but there may be a slight shift of the sidelobe positions.

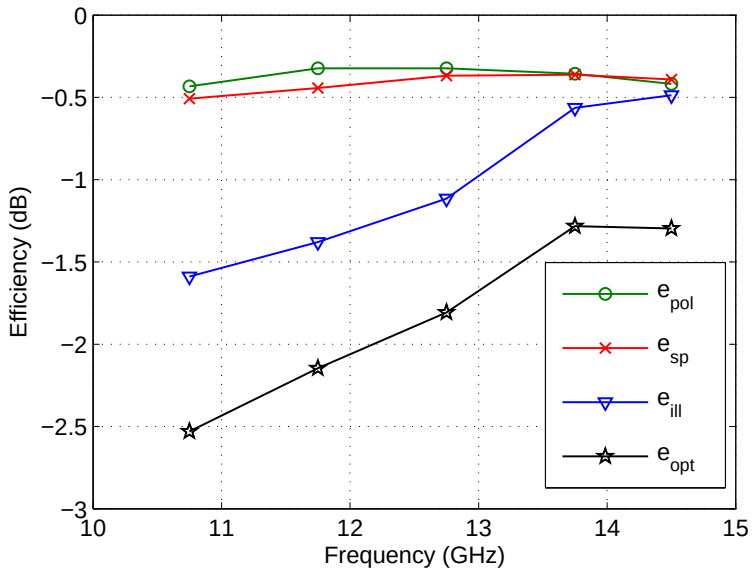

Figure 6.9: Simulated feed efficiencies with e_{opt} being the sum of the sub efficiencies.

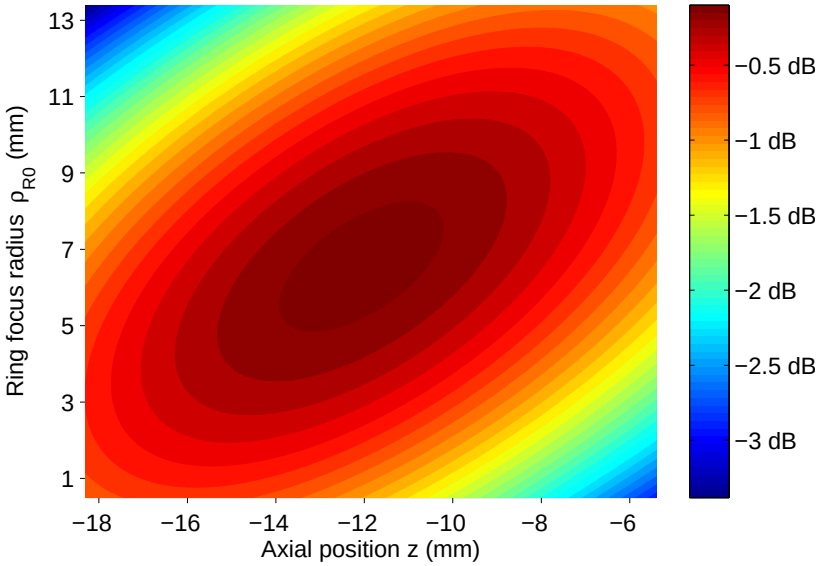

Figure 6.10: Phase efficiency of the optimized hat feed for different ring radii ρ_R and phase reference locations z.

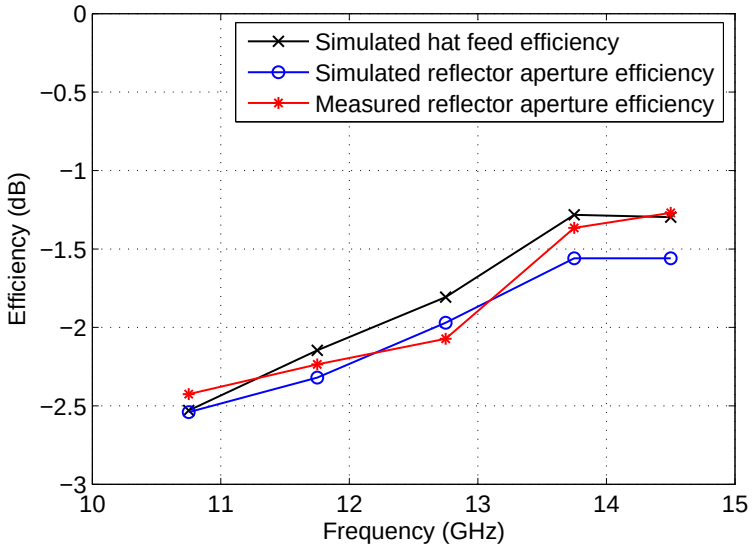

Figure 6.11: Simulated and measured aperture efficiency of the hat-fed reflector antenna and simulated hat feed efficiency.

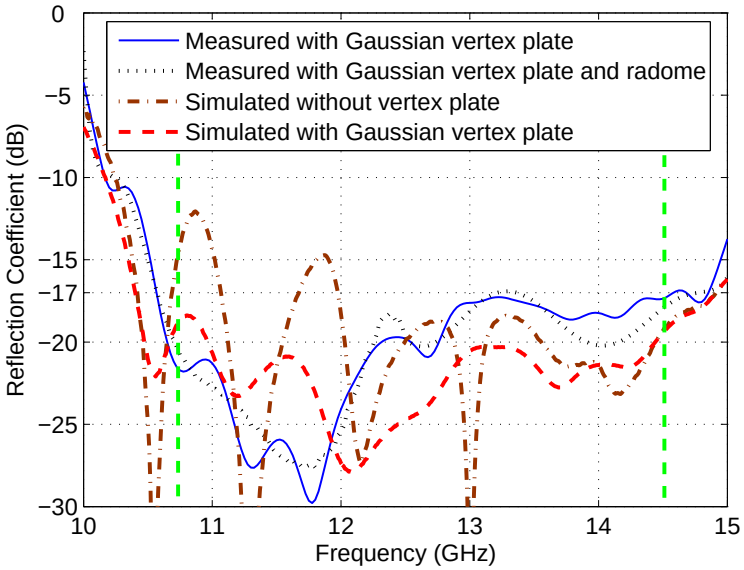

Figure 6.12: Simulated and measured reflection coefficient of the hat-fed reflector antenna with and without the Gaussian vertex plate, and with the radome.

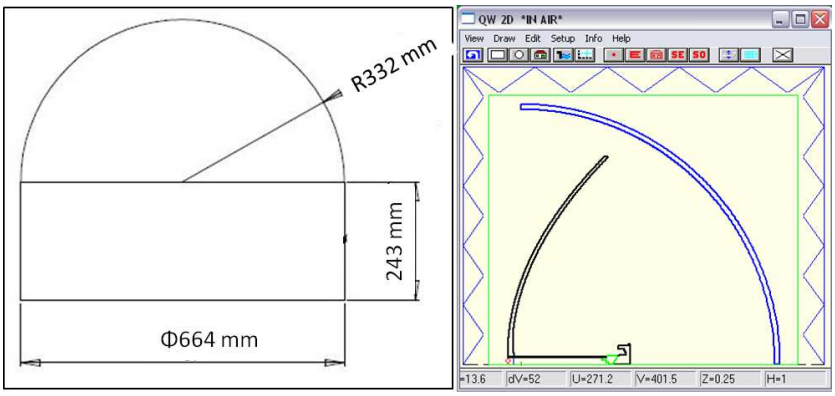

Figure 6.13: The radome outer dimensions and the QW-V2D model of the hat-fed reflector antenna enclosed by a hemispherical radome.

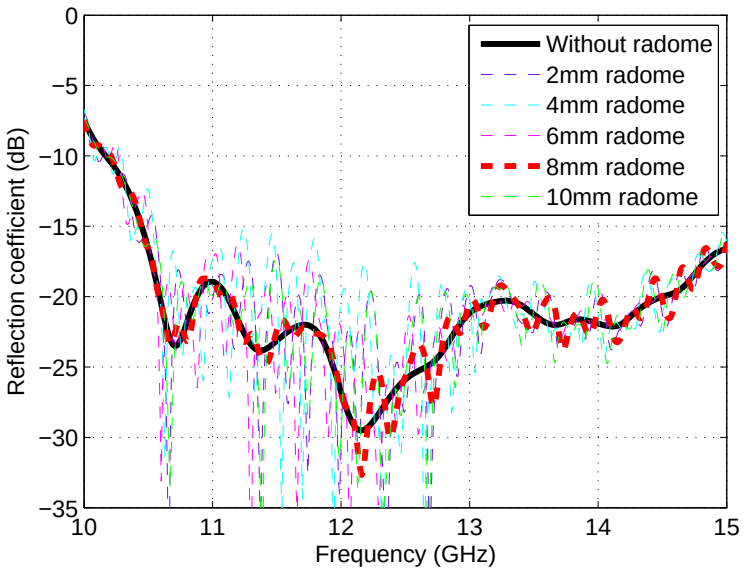

Figure 6.14: Simulated reflection coefficient of the hat-fed reflector antenna enclosed by a radome of various thickness.

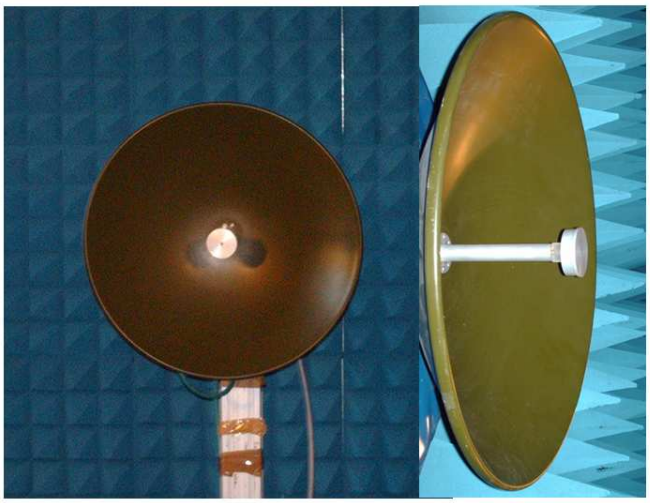

Figure 6.15: Hat-fed reflector antenna under test in anechoic chamber.

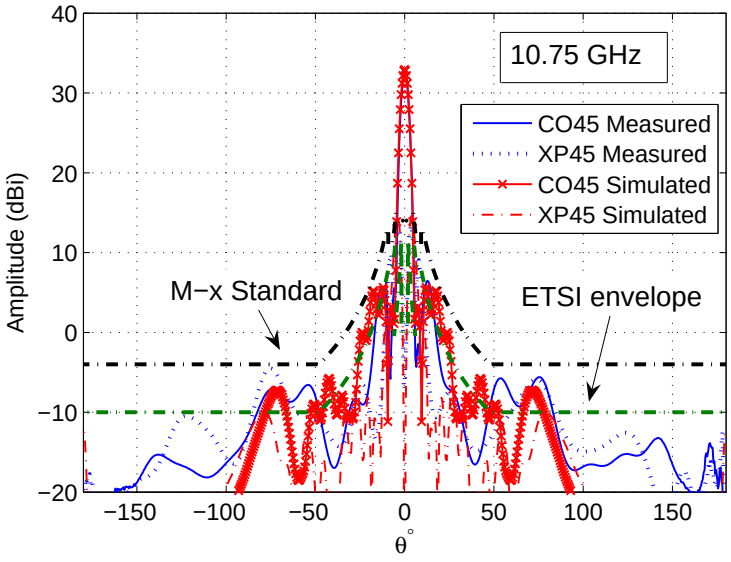

Figure 6.16: Radiation patterns of hat-fed reflector antenna in the $\varphi = 45°$ plane with sidelobe envelopes at 10.75 GHz.

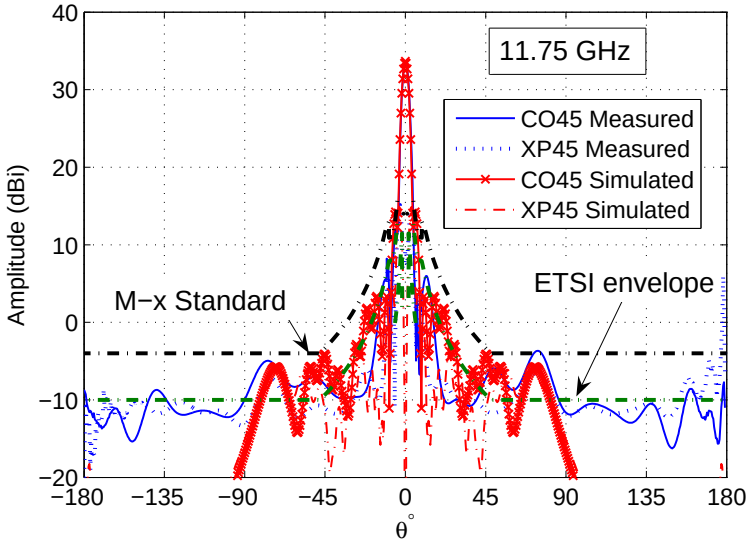

Figure 6.17: Radiation patterns of hat-fed reflector antenna in the $\varphi = 45°$ plane with sidelobe envelopes at 11.75 GHz.

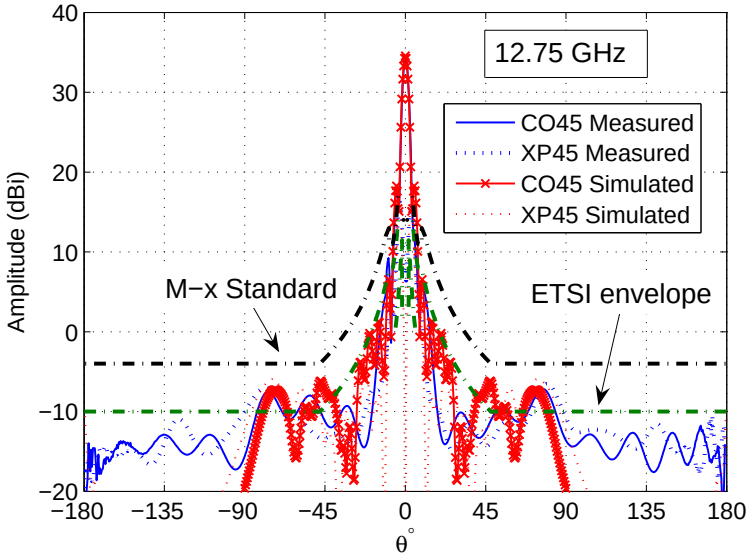

Figure 6.18: Radiation patterns of hat-fed reflector antenna in the $\varphi = 45°$ plane with sidelobe envelopes at 12.75 GHz.

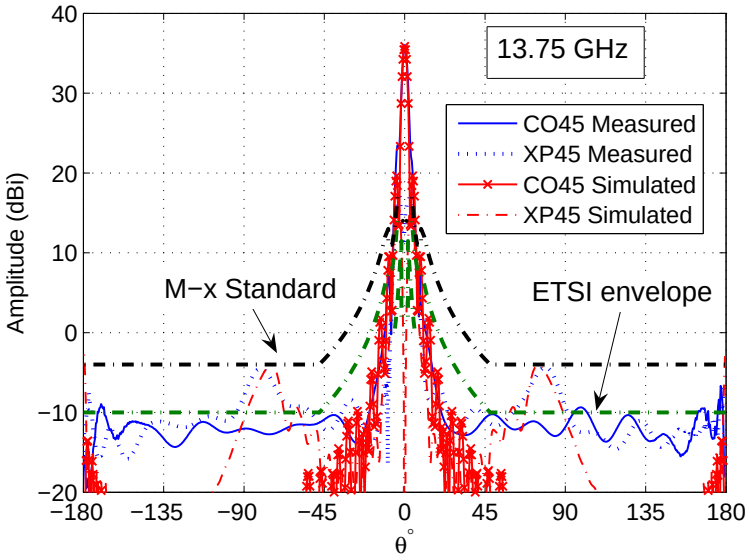

Figure 6.19: Radiation patterns of hat-fed reflector antenna in the $\varphi = 45°$ plane with sidelobe envelopes at 13.75 GHz.

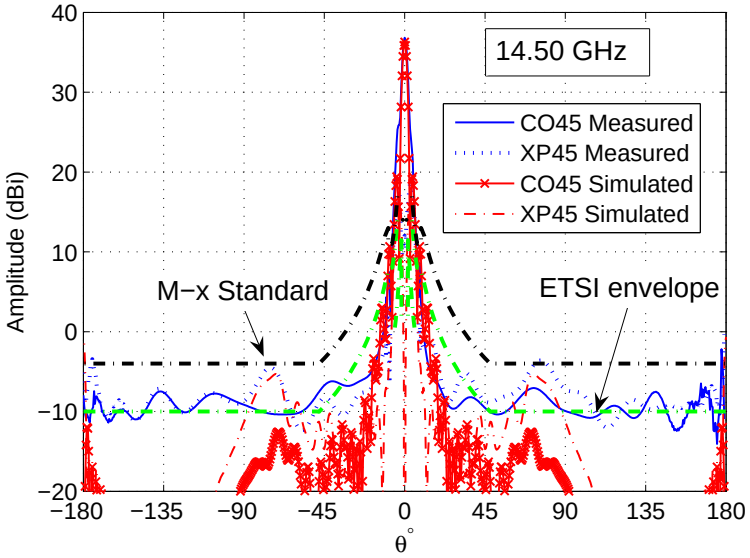

Figure 6.20: Radiation patterns of hat-fed reflector antenna in the $\varphi = 45°$ plane with sidelobe envelopes at 14.50 GHz.

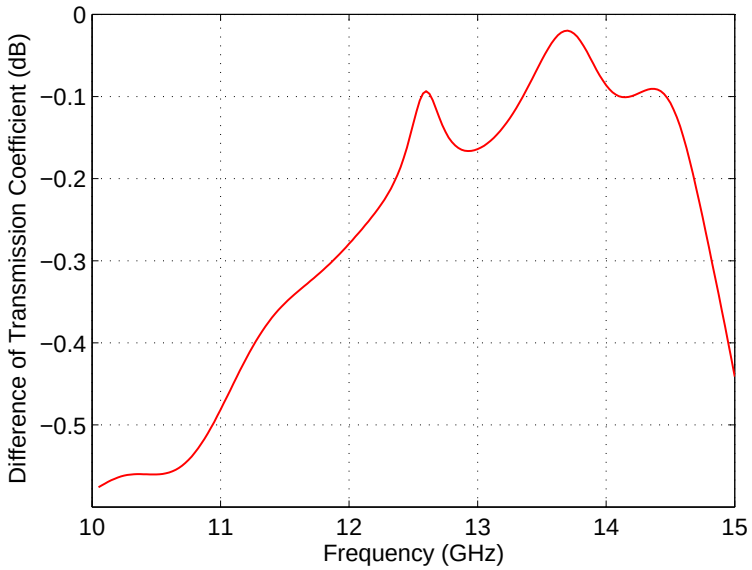

Figure 6.21: Measured difference of the transmission coefficients between two conical horns separated by 7.14 mm in the case of radome and no radome in between. S_{21} of radome case measurement subtracted from S_{21} of no radome case.

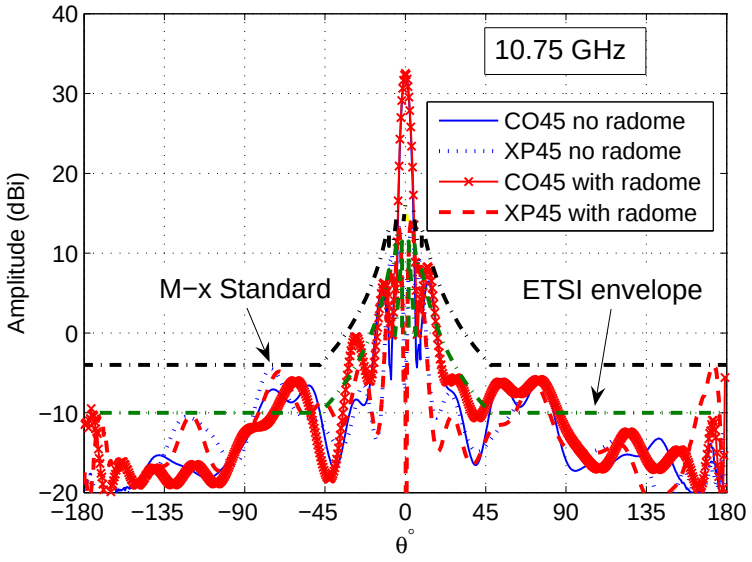

Figure 6.22: Measured radiation patterns of hat-fed reflector antenna in the $\varphi = 45°$ plane at 10.75 GHz with and without radome. Sidelobe envelopes included.

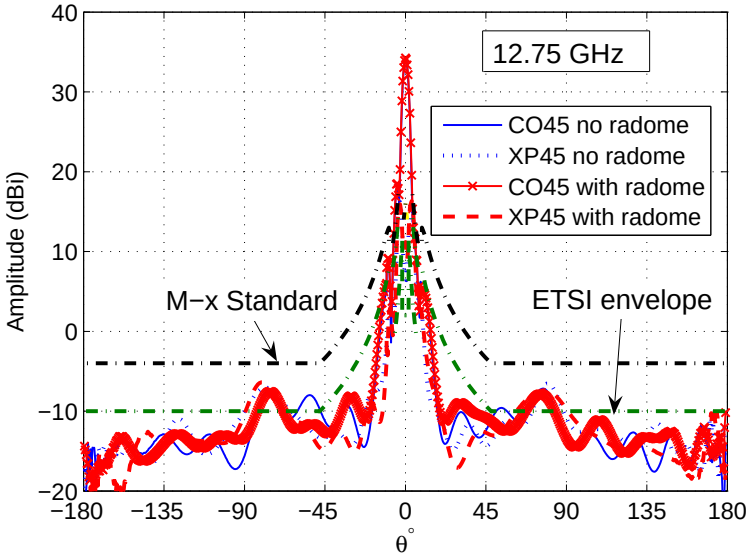

Figure 6.23: Measured radiation patterns of hat-fed reflector antenna in the $\varphi = 45°$ plane at 12.75 GHz with and without radome. Sidelobe envelopes included.

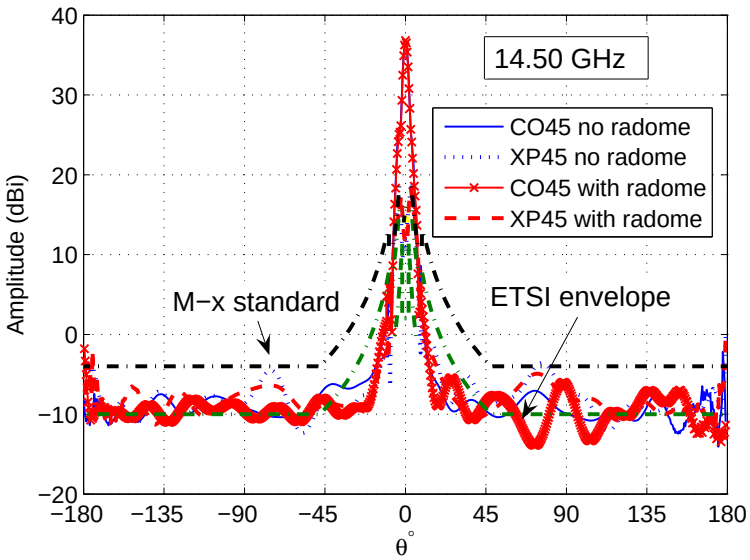

Figure 6.24: Measured radiation patterns of hat-fed reflector antenna in the $\varphi = 45°$ plane at 14.50 GHz with and without radome. Sidelobe envelopes included.

Chapter 7

Conclusions and Future Work

7.1 Conclusions

In this thesis we have taken a practical approach in the developed of a hat-fed reflector antenna with radome for satellite earth station. Emphasis has been on: 1) Implementation of genetic algorithm for optimization of reflection coefficient and feed efficiency; 2) Study and implementation of Gaussian vertex plate for minimized reflection coefficient; 3) Study of optimum shaped ring focus reflector; 4) Sidelobe suppression of antenna radiation patterns to comply with standards for satellite communication; 5) Analysis and design of radome structures. Measurements have shown that the satellite earth terminal comply with the M-x standard and can be operational.

7.2 Future Work

Further development includes implementation of monopulse tracking functionality in the hat feed by exciting the TE_{21} mode. The antenna can also be designed for dual band applications including the Ka-satcom-band. Furthermore, the optimization procedure may be extended to include reflector antenna radiation patterns to meet the most stringent ETSI sidelobe requirements.

References

[1] H. Noordung, "The problem of space travel," *The NASA history series*, vol. SP-4026, 1995.

[2] A. C. Clarke, "The Future of World Communications - Extra Terrestrial Relays," *Wireless World Mag.*, no. 10, pp. 305–308, 1945.

[3] B. R. Elbert, *Introduction to Satellite Communication*, 3rd ed. Artech House, Inc., 2008, ch. 1.

[4] M. Denstedt, T. Östling, J. Yang, and P.-S. Kildal, "Tripling bandwidth of hat feed by genetic algorithm optimization." presented at the IEEE Int. Symp. on Antennas Propagat., Honolulu, HI, 10-15 June 2007.

[5] E. Geterud, J. Yang, and T. Östling, "Wide band hat-fed reflector antenna for satellite communications." presented at the 5th Eur. Conf. on Antennas Propagat., Rome, IT, 11-15 April 2011.

[6] E. Geterud, J. Yang, T. Östling, and B. P., "Design and optimization of compact wideband hat-fed reflector antenna for satellite communications," *IEEE Trans. Antennas Propagat., to be published.*

[7] E. Geterud, J. Yang, and T. Östling, "Radome design for hat-fed reflector antenna." presented at the 6th Eur. Conf. on Antennas Propagat., Prague, CZ, 26-30 March 2012.

[8] C. C. Cutler, "Parabolic-antenna design for microwaves," *in Proc. of the IRE*, vol. 35, no. 11, pp. 1284–1294, 1947.

[9] P.-S. Kildal, *Foundations of Antennas a Unified Approach*, 1st ed. Studentlitteratur, 2000, ch. 8.

[10] ——, "The hat feed: a dual-mode rear-radiating waveguide antenna having low cross polarization," *IEEE Trans. Antennas Propagat.*, vol. 35, no. 9, pp. 1010–1016, 1987.

[11] J. Yang and P.-S. Kildal, "FDTD design of a Chinese hat feed for shallow mm-wave reflector antennas." in Proc. of the IEEE AP-S Int. Symp., 1998, pp. 2046–2049.

[12] C. Granet, "Designing axially symmetric Cassegrain or Gregorian dual-reflector antennas from combination of prescribed parameters," *IEEE Antennas and Propagat. Mag.*, vol. 40, no. 2, pp. 76–82, 1998.

[13] ——, "A simple procedure for the design of classical displaced axis dual-reflector antennas using a set of geometric parameters," *IEEE Antennas and Propagat. Mag.*, vol. 41, no. 6, pp. 64–71, 1999.

[14] R. C. Byrd, "Photo of green bank telescope," July 2012. [Online]. Available: $http://atomictoasters.com/2012/03/big-complicated-machines-12-the-green-bank-telescope/$

[15] A. D. Olver, P. J. B. Clarricoats, A. A. Kishk, and L. Shafai, *Microwave Horns and Feeds*, 1st ed. IEEE Press, 1994, ch. 1.

[16] C. A. Balanis, *Modern Antenna Handbook*, 1st ed. John Wiley and Sons, Inc., 2008, ch. 12.

[17] D. Valderas, J. I. Sancho, D. Puente, C. Ling, and X. Chen, *Ultra wideband antennas, Design and applications*, 1st ed. Imperial College Press, 2011, ch. 3.

[18] R. Olsson, P.-S. Kildal, and S. Weinreb, "The Eleven antenna: A compact low-profile decade bandwidth dual polarized feed for reflector antennas," *IEEE Trans. Antennas Propagat.*, vol. 54, no. 2, pp. 368–375, 2005.

[19] J. Yang, M. Pantaleev, P.-S. Kildal, and L. Hellner, "Design of compact dual-polarized 1.2-10 GHz Eleven feed for decade bandwidth radio telescopes," *IEEE Trans. Antennas Propagat.*, vol. 60, no. 5, pp. 2210–2218, 2012.

[20] J. Yang, M. Pantaleev, P.-S. Kildal, B. Klein, Y. Karadikar, L. Helldner, N. Wade-falk, and C. Beaudoin, "Cryogenic 2-13 GHz Eleven feed for reflector antennas in future wideband radio telescopes," *IEEE Trans. Antennas Propagat.*, vol. 59, no. 6, pp. 1918–1934, June 2011.

[21] J. Yin, J. Yang, M. Pantaleev, and L. Helldner, "The circular Eleven antenna: a new decade-bandwidth feed for reflector antennas with a high aperture efficiency," *IEEE Trans. Antennas Propagat., to be published.*

[22] P.-S. Kildal and E. Lier, "Hard horns improve cluster feeds of satellite antennas," *Electronics Letters*, vol. 24, no. 8, pp. 491–492, 1988.

[23] Finmeccanica, "Photo of 3D multi-role C-band phased array antenna radar," July 2012. [Online]. Available: *http* : *//www.flickr.com/photos/finmeccanica/*5887989166*/in/photostream*

[24] ETSI, "Satellite Earth Stations and Systems (SES) Harmonized EN for Very Small Aperture Terminal (VSAT)," ETSI EN 301 428 V1.3.1, Tech. Rep., Feb. 2006.

[25] Eutelsat, "Conditions of operations of earth stations not fully complying with standard M. Nomenclature of standard M-x." Addendum to EESS 502. Issue 1, Rev.1, Tech. Rep., Oct. 2008.

[26] P.-S. Kildal and Z. Sipus, "Classification of rotationally symmetric antennas as types BOR_0 and BOR_1," *IEEE Trans. Antennas Propagat.*, vol. 37, no. 6, pp. 114–117, 1995.

[27] QWED, "QW-V2D Software for Electromagnetic Design," July 2012. [Online]. Available: *http* : *//www.qwed.com.pl/qw_v*2*d.html*

[28] W. Gwarek, K. Morawski, and C. Mroczkowski, "Application of the FD-TD method to the analysis of circuits described by the two-dimensional vector wave equation," *IEEE Trans. Microwave Theory Tech.*, vol. 41, no. 2, pp. 311–317, 1992.

[29] Y. Rahmat-Samii and E. Michielssen, *Electromagnetic Optimization by Genetic Algorithm*, 1st ed. John Wiley and Sons, Inc., 1999, ch. 1.

[30] G. C. Onwubolu and B. V. Babu, *New Optimization Techniques in Engineering*, 1st ed. Springer-Verlag, 2004, ch. 8.

[31] S. S. Rao, *Engineering Optimization*: *Theory and Practice*, 4th ed. John Wiley and Sons, Inc., 2009, ch. 6.

[32] X.-S. Yang, *Engineering Optimization*: *An introduction with metaheuristic applications*, 1st ed. John Wiley and Sons, Inc., 2010, ch. 10.

[33] J. Yang and P.-S. Kildal, "Algorithm and modeling for fast optimization and design of large log-periodic array antennas with commercial EM solvers," vol. 33, no. 12. in Proc. of the 5th Eur. Conf. on Antennas and Propagat., 2011, pp. 3946–3949.

[34] ——, "Optimization of reflection coefficient of large log-periodic array by computing only a small part of it," *IEEE Trans. Antennas Propagat.*, vol. 59, no. 6, pp. 1790–1797, June 2011.

[35] P.-S. Kildal and A. Nyseth, "The hat feed: A new typ of splash plate antenna having low cross polarization," *IEEE Antennas Propagat. SOC. Int. Symp. Dig.*, vol. 1, no. 1, pp. 75–78, 1986.

[36] P.-S. Kildal, "Artificially soft and hard surfaces in electromagnetics," *IEEE Trans. Antennas Propagat.*, vol. 38, no. 10, pp. 1537–1544, 1990.

[37] W. Wei, Y. Yang, T. Östling, and T. Schafer, "A new hat feed for reflector antennas realized without dielectrics for reducing manufacturing cost and improving reflection coefficient," *IET Microwaves Antennas Propagat.*, vol. 5, no. 7, pp. 837–843, July 2011.

[38] J. Yang and P.-S. Kildal, "Calculation of ring-shaped phase centers of feeds for ring-focus paraboloids," *IEEE Trans. Antennas Propagat.*, vol. 48, no. 4, pp. 524–528, 2000.

[39] P.-S. Kildal, "Improved reflector antenna with self supported feed," Patent US 6 137 449, Oct. 24, 2000.

[40] ——, "A small dipole-fed resonant reflector antenna with high efficiency, low cross polarizaton and low sidelobes," *IEEE Trans. Antennas Propagat.*, vol. 33, no. 12, pp. 1386–1391, 1985.

[41] A. Moldsvor and P.-S. Kildal, "Systematic approach to control feed scattering and multiple reflections in symmetrical primary-fed reflector antennas," vol. 139. in IEE Proc., Sept. 1992, pp. 65–71.

[42] J. Yang and P.-S. Kildal, "Gaussian vertex plate improves reflection coefficient and far-out sidelobes in prime-focus reflector antennas," *Microwave and Optical Tech. Lett.*, vol. 21, no. 2, pp. 125–129, 1999.

[43] P.-S. Kildal, A. Skyttemyr, and A. Kishk, "G/T maximization of a paraboidal reflector fed by a dipole-disk antenna with ring by using the multple-reflection approach and the moment method," *IEEE Trans. Antennas Propagat.*, vol. 47, no. 7, pp. 1130–1139, 1997.

[44] A. C. Ludwig, "Antenna feed efficiency," *Space Programs Summary*, vol. 37-26, no. 6, pp. 200–208, 1965.

[45] P.-S. Kildal, "Factorization of the feed efficiency of paraboloids and cassegrain antennas," *IEEE Trans. Antennas Propagat.*, vol. 33, no. 8, pp. 903–908, 1985.

[46] D. J. Kozakoff, *Analysis of Radome Enclosed Antennas*, 2nd ed. Artech House, Inc., 2009, ch. 1.

[47] Skycom, "Photo of radome enclosing parabolic antenna," July 2012. [Online]. Available: *http* : *//www.skycom.co.uk/wbur.html*

[48] W. S. Weiglhofer and A. Lakhtakia, *Introduction to Complex Mediums for Electromagnetics and Optics*, 1st ed. SPIE Publications, 2003, ch. 1.

[49] H. N. Liu, "Design of antenna radome composed of metamaterials for high gain," *IEEE Antennas Propagat. SOC. Int. Symp. Dig.*, vol. 1, no. 1, pp. 19–22, 2006.